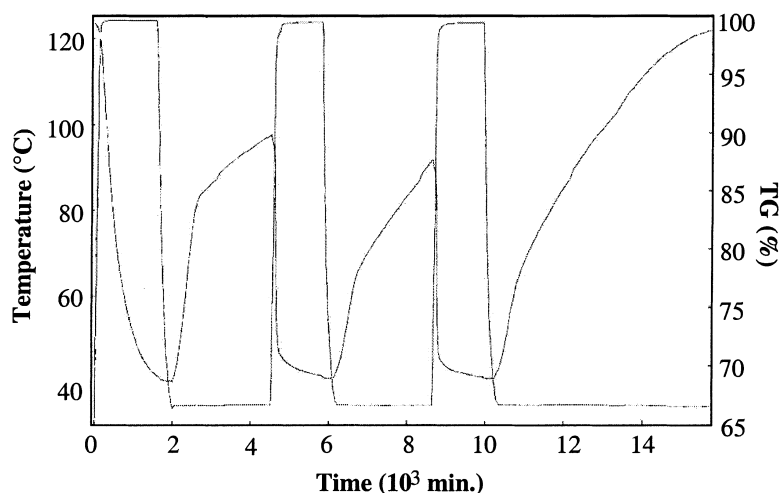


1,4-Dioxobenzene Compounds of Gallium: Reversible Binding of Pyridines to $[(Bu)Ga](\eta\text{-OCHO})$ in the Solid State

Laura H. van Poppel, Simon G. Bott, and Andrew R. Barron

J. Am. Chem. Soc., **2003**, 125 (36), 11006-11017 • DOI: 10.1021/ja0208714

Downloaded from <http://pubs.acs.org> on January 12, 2009



More About This Article

Additional resources and features associated with this article are available within the HTML version:

- Supporting Information
- Links to the 2 articles that cite this article, as of the time of this article download
- Access to high resolution figures
- Links to articles and content related to this article
- Copyright permission to reproduce figures and/or text from this article

[View the Full Text HTML](#)

1,4-Dioxobenzene Compounds of Gallium: Reversible Binding of Pyridines to $[(\text{tBu})_2\text{Ga}]_2(\mu\text{-OC}_6\text{H}_4\text{O})_n$ in the Solid State

Laura H. van Poppel,[†] Simon G. Bott,[‡] and Andrew R. Barron^{*,†,§}

Contribution from the Department of Chemistry and Center for Nanoscale Science and Technology, Rice University, Houston, Texas 77005 and Department of Chemistry, University of Houston, Houston, Texas 77204

Received June 21, 2002; E-mail: arb@rice.edu

Abstract: The gallium aryloxide polymer, $[(\text{tBu})_2\text{Ga}]_2(\mu\text{-OC}_6\text{H}_4\text{O})_n$ (**1**) is synthesized by the addition of $\text{Ga}(\text{tBu})_3$ with hydroquinone in a noncoordinating solvent, and reacts with pyridines to yield the yellow compound $[(\text{tBu})_2\text{Ga}(\text{L})]_2(\mu\text{-OC}_6\text{H}_4\text{O})$ [$\text{L} = \text{py}$ (**2**), 4-Mepy (**3**), and 3,5-Me₂py (**4**)] via cleavage of the Ga_2O_2 dimeric core. The analogous formation of $\text{Ga}(\text{tBu})_2(\text{OPh})(\text{py})$ (**5**) occurs by dissolution of $[(\text{tBu})_2\text{Ga}(\mu\text{-OPh})]_2$ in pyridine. In solution, **2–4** undergo dissociation of one of the pyridine ligands to yield $[(\text{tBu})_2\text{Ga}(\text{L})(\mu\text{-OC}_6\text{H}_4\text{O})\text{Ga}(\text{tBu})_2]_2$, for which the ΔH and ΔS have been determined. Thermolysis of compounds **2–4** in the solid-state results in the loss of the Lewis base and the formation of **1**. The reaction of **1** or $[(\text{tBu})_2\text{Ga}(\mu\text{-OPh})]_2$ with the vapor of the appropriate ligand results in the solid state formation of **2–4** or **5**, respectively. The ΔH^\ddagger and ΔS^\ddagger for both ligand dissociation and association for the solid–vapor reactions have been determined. The interconversion of **1** into **2–4**, as well as $[(\text{tBu})_2\text{Ga}(\mu\text{-OPh})]_2$ into **5**, and their reverse reactions, have been followed by ¹³C CPMAS NMR spectroscopy, TG/DTA, SEM, EDX, and powder XRD. Insight into this solid-state polycondensation polymerization reaction may be gained from the single-crystal X-ray crystallographic packing diagrams of **2–5**. The crystal packing for compounds **2**, **3**, and **5** involve a head-to-head arrangement that is maintained through repeated ligand dissociation and association cycles. In contrast, when compound **4** is crystallized from solution a head-to-tail packing arrangement is formed, but during reintroduction of 3,5-Me₂py in the solid state–vapor reaction of compound **1**, a head-to-head polymorph is postulated to account for the alteration in the ΔH^\ddagger of subsequent ligand dissociation reactions. Thus, the ΔH^\ddagger for the condensation polymerization reaction is dependent on the crystal packing; however, the subsequent reversibility of the reaction is dependent on the polymorph.

Introduction

Although aimed at different functions, chemical sensors,¹ and chemically triggered switches^{2,3} have certain underlying principles in common. First, each must contain active sites or functional groups that bind or trap a guest molecule. Second, when a host–guest interaction occurs, it must be accompanied by some physical change, e.g., color,⁴ conductivity,⁵ or luminescence.⁶ Third, the host–guest interaction should function in a reversible fashion, ideally without degradation of the host.

The interaction between host and guest may be accomplished in a number of ways; however, two general approaches have been studied in detail. By changing (tailoring) the size and shape of molecular cavities in host compounds, inclusion compounds, such as zeolites and calixarenes, have been made to trap specific molecules or ions. Alternatively, the molecules may be involved in specific chemical binding. For example, hydrogen bonding often plays a role in inclusion compounds' ability to trap solvent molecules.⁷ The formation of a specific bonding interaction between a host and guest has generally been limited to spatially controlled hydrogen bonding networks or Lewis acid–base interactions. The latter ordinarily requires a vacant coordination site on a metal center⁸ or the ability of the metal to expand its coordination sphere.⁹ A combination of these approaches is often employed.

[†] Rice University.

[‡] University of Houston.

[§] URL: www.rice.edu/barron.

- (1) *Sensors A Comprehensive Survey*; Göpel, W., Jones, T. A., Kleitz, M., Lundström, J., Seiyama, T., Eds.; VCH: New York, 1991; Vol. 2, Chemical and Biochemical Sensors Part I.
- (2) (a) Sugimoto, H.; Kimura, T.; Inoue, S., *J. Am. Chem. Soc.* **1999**, *121*, 2325. (b) Matthews, O. A.; Raymo, F. M.; Stoddart, J. F.; White, A. J. P.; Williams, D. J. *New J. Chem.* **1998**, *22*, 1131.
- (3) Pease, A. R.; Jeppesen, J. O.; Stoddart, J. F.; Luo, Y.; Collier, C. P.; Heath, J. R. *Acc. Chem. Res.* **2001**, *34*, 433.
- (4) (a) Zusman, R.; Rottman, C.; Ottolenghi, M.; Avnir, D. *J. Non-Cryst. Solids* **1990**, *122*, 107. (b) Dunn, B.; Zink, J. I. *J. Mater. Chem.* **1991**, *1*, 903.
- (5) (a) Murakami, T. I. *Anal. Lett.* **1986**, *19*, 1973. (b) Gotoh, M.; Tamiya, E.; Karube, I.; Kagawa, Y. *Anal. Chim. Acta* **1986**, *187*, 287. (c) Wu, S.; Li, F.; Zhu, Y.; Shen, J. *J. Mater. Sci.* **2000**, *35*, 2005. (d) Steenwinkel, P.; Grove, D. M.; Veldman, N.; Spek, A. L.; van Koten, G. *Organometallics* **1998**, *17*, 5647. (e) Ding, H.; Erokhin, V.; Ram, M. K.; Paddeu, S.; Valkova, L.; Nicolini, C. *Thin Solid Films* **2000**, *379*, 279.

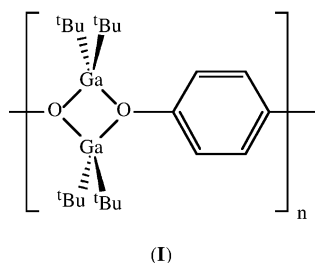
- (6) (a) Winder, E. J.; Moore, D. E.; Neu, D. R.; Ellis, A. B.; Geisz, J. F.; Kuech, T. F. *J. Cryst. Growth* **1995**, *148*, 63. (b) Geisz, J. F.; Kuech, T. F.; Ellis, A. B. *J. Appl. Phys.* **1995**, *77*, 1233. (c) Glass, T. E. *J. Am. Chem. Soc.* **2000**, *122*, 4522.
- (7) Meinhold, D.; Seichter, W.; Köhnke, K.; Seidel, J.; Weber, E. *Adv. Mater.* **1997**, *9*, 958.
- (8) (a) Albrecht, M.; Lutz, M.; Spek, A. L.; van Koten, G. *Nature* **2000**, *406*, 970. (b) Albrecht, M.; Lutz, M.; Schreurs, A. M. M.; Lutz, E. T. H.; Spek, A. L.; van Koten, G. *J. Chem. Soc., Dalton Trans.* **2000**, 3797.
- (9) Bourne, S. A.; Kilkenny, M.; Nassimbeni, L. R. *J. Chem. Soc., Dalton Trans.* **2001**, 1176.

Group 13 alkoxides are known to form dimeric compounds with the general formula $[R_2M(\mu-OR')]_2$ ($M = Al, Ga, In$).¹⁰ With the addition of a Lewis base, this M_2O_2 core can be cleaved, and monomeric compounds can be observed in solution in equilibrium with the dimeric species. With more sterically bulky R' groups, monomeric compounds have been isolated and characterized.¹¹ Despite various kinetic and thermodynamic measurements for these reactions in solution, and the determination of dissociation energies in vapor phase, there has been a paucity of studies on solid–vapor reactions. With this in mind, a polymeric gallium aryloxide polymer $[\{(tBu)_2Ga\}_2(\mu-OC_6H_4O)]_n$ has been synthesized in which a Ga_2O_2 core is cleaved by a strong Lewis base to afford a monomeric species in solution, as well as in the solid state. This gallium aryloxide polymer also exhibits the characteristics of a molecular sensor and/or switch, where the polymer acts as a “host” to pyridine (the “guest”), but instead of relying on a vacant coordination site, the Lewis base cleavage of a Ga_2O_2 core is the key for the host–guest interaction.

Results and Discussion

The gallium aryloxide polymer, $[\{(tBu)_2Ga\}_2(\mu-OC_6H_4O)]_n$ (**1**), is synthesized by the addition of $Ga(tBu)_3$ to hydroquinone at $-78\text{ }^\circ\text{C}$ in a noncoordinating solvent. Elemental analysis and mass spectra fragmentation patterns are consistent with this formulation. Compound **1** is stable in air for short periods of time and is insoluble in solvents in which it does not react.

The ^{13}C CPMAS NMR of compound **1** (see the Experimental section) shows only a single resonance for each carbon environment concordant with a highly symmetrical species in which the 1,4-dioxobenzene ligand is bridging. The chemical shifts for the *tert*-butyl groups and the aryl carbons of the polymer are similar to the equivalent peaks found for the phenoxide dimer, $[(tBu)_2Ga(\mu-OPh)]_2$, see the Experimental section, suggesting a similar structure. We have previously shown that the ^{13}C NMR shift for the alkyl substituents on Group 13 metals is dependent on the coordination number around the metal.¹² The ^{13}C CPMAS NMR shift for the *tert*-butyl in compound **1** ($\delta = 32.7$ ppm) is within the range previously observed for dimeric gallium aryloxide compounds, $[(tBu)_2Ga(\mu-OR)]_2$, ($\delta = 30.7\text{--}32.9$ ppm),¹³ and distinct from the analogous shift in three-coordinate gallium alkoxides, e.g., $\delta = 28.98$ ppm for $(tBu)_2Ga(OCPh_3)$.¹⁴ On this basis, we propose that the gallium aryloxide polymer has a Ga_2O_2 dimeric core (**I**) and structure typically observed for gallium alkoxides.¹⁵



Compound **1** is insoluble in noncoordinating solvents; however, coordinating solvents, such as THF, MeCN, and

pyridines allow for the dissolution of **1**. Only the products from the interactions with pyridine, 4-picoline (4-Mepy), and 3,5-lutidine (3,5-Me₂py) have been characterized; however, based on the ^1H and ^{13}C NMR spectra of compound **1** dissolved in d_8 -THF and d_3 -MeCN, similar species are formed with these Lewis bases. A similar reaction has been previously reported for aluminum 1,4-dioxybenzene compounds.^{16,17}

Dissolution of compound **1** in pyridine (or methyl substituted pyridine) results in cleavage of the Ga_2O_2 dimeric core and yields the yellow monomeric compound $[(tBu)_2Ga(L)]_2(\mu-OC_6H_4O)$, where $L = \text{py}$ (**2**), 4-Mepy (**3**), and 3,5-Me₂py (**4**). Compounds **2–4** may also be prepared by the direct reaction of $Ga(tBu)_3$ with hydroquinone in the presence of pyridine, 4-Mepy or 3,5-Me₂py, respectively. The aluminum analogues of compounds **2** and **4**, as well as the THF complex have been isolated.¹⁷ Compounds **2–4** have been characterized by solution and solid-state NMR spectroscopy and single-crystal X-ray diffraction. In addition, crystals of compound **2** grown from pyridine solution contain a solvent of crystallization of pyridine, i.e., **2**.py. The analogous formation of $Ga(tBu)_2(OPh)(\text{py})$ (**5**) by dissolution of $[(tBu)_2Ga(\mu-OPh)]_2$ in pyridine (see the Experimental section) further supports the proposed structure of compound **1**.

The solid-state structure of compounds **2–4** are shown in Figure 1; selected bond lengths and angles are given in Table 1. The centrosymmetric molecular structures consist of a 1,4-dioxobenzene ligand bridging two $Ga(tBu)_2(L)$ moieties, with all bond lengths and angles within the ranges for related compounds.¹⁸ The gallium atoms are positioned on either side of the plane of the 1,4-dioxobenzene ligand. This is in contrast to the solid-state structure of the mono-gallium phenoxide analogue, $Ga(tBu)_2(OPh)(\text{py})$ (**5**) (Table 1) in which the pyridine and phenoxide ligands are coplanar (Figure 2). The presence of a pyridine of solvation in **2**.py does not appear to significantly affect the structure, see Table 1.

As is common with other gallium aryloxides, compounds **2–4** are moisture sensitive, but only slightly air sensitive. Each compound is soluble in its respective Lewis base, and also sparingly soluble in C_6H_6 and $CHCl_3$. Unlike compound **1**, the Lewis base adducts are yellow in color showing two absorptions at 302–303 and 327–329 nm (see the Experimental section) which may be assigned to a ligand-to-ligand charge transfer from a $Ga-C_\sigma$ to the low lying π^* orbital of the pyridine.¹⁹

Ligand Dissociation in Solution. The solution ^1H and ^{13}C NMR spectra of compounds **2–4** shows two sets of resonances; the first can be assigned to $[(tBu)_2Ga(L)]_2(\mu-OC_6H_4O)$, whereas

- (12) (a) Barron, A. R. *J. Chem. Soc., Dalton Trans.* **1988**, 3047. (b) Rogers, J. H.; Applett, A. W.; Cleaver, W. M.; Tyler, A. N.; Barron, A. R. *J. Chem. Soc., Dalton Trans.* **1992**, 3179.
- (13) Cleaver, W. M.; Barron, A. R.; McGuffey, A. R.; Bott, S. G. *Polyhedron* **1994**, *13*, 2831.
- (14) Cleaver, W. M.; Barron, A. R. *Organometallics* **1993**, *12*, 1001.
- (15) (a) Dembowski, U.; Pape, T.; Herbst-Irmer, R.; Pohl, E.; Roesky, H. W.; Sheldrick, G. M. *Acta Cryst.* **1993**, *C49*, 1309. (b) Keys, A.; Barbarich, T.; Bott, S. G.; Barron, A. R. *J. Chem. Soc., Dalton Trans.* **2000**, 577.
- (16) Kaul, F. A. R.; Tschinkl, M.; Gabbai, F. P. *J. Organomet. Chem.* **1997**, *539*, 187.
- (17) van Poppel, L. H.; Bott S. G.; Barron, A. R. *J. Chem. Soc., Dalton Trans.* **2002**, 3327.
- (18) Tuck, D. G. *Comprehensive Organometallic Chemistry*; Wilkinson, G., Stone, F. G. A., Abel, E. W., Eds.; Pergamon Press: Oxford, 1982; Vol. 1, Ch. 7.
- (19) (a) Beumgarten, J.; Bessenbacher, C.; Kaim, W.; Stahl, T. *J. Am. Chem. Soc.* **1989**, *111*, 2126. (b) Lichtenberger, D. L.; Hogan, R. H.; Healy, M. D.; Barron, A. R. *Organometallics* **1991**, *10*, 609. (c) Mason, M. R.; Smith, J. M.; Bott, S. G.; Barron, A. R. *J. Am. Chem. Soc.* **1993**, *115*, 4971.

(10) Healy, M. D.; Ziller, J. W.; Barron, A. R. *Organometallics* **1991**, *10*, 597.
 (11) Healy, M. D.; Power, M. B.; Barron, A. R. *Coord. Chem. Rev.* **1994**, *94*, 63.

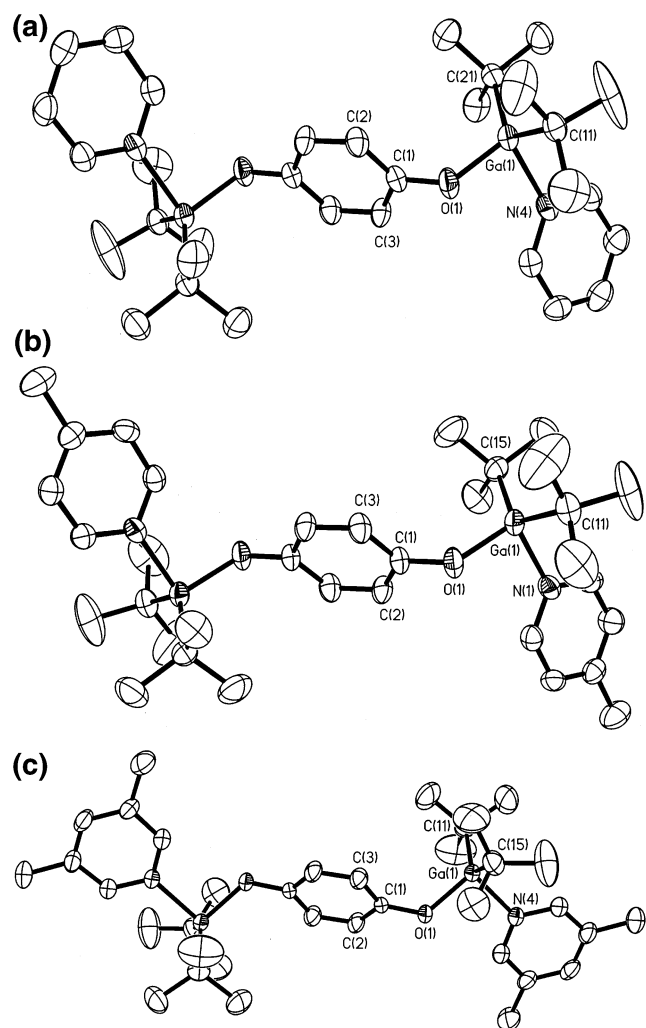


Figure 1. Molecular structures of (a) [(*t*Bu)₂Ga(py)]₂(μ-OC₆H₄O) (**2**), (b) [(*t*Bu)₂Ga(4-Mepy)]₂(μ-OC₆H₄O) (**3**) and (c) [(*t*Bu)₂Ga(3,5-Me₂py)]₂(μ-OC₆H₄O) (**4**). Thermal ellipsoids shown at the 30% level, and hydrogen atoms are omitted for clarity.

the second is consistent with dissociation of one of the Lewis base ligands per di-gallium unit, and the formation of the dimers [(*t*Bu)₂Ga(L)(μ-OC₆H₄O)Ga(*t*Bu)₂]₂ (**II**). A similar structure has been previously reported for dimethylaluminum 1,4-dioxybenzene compounds.¹⁶

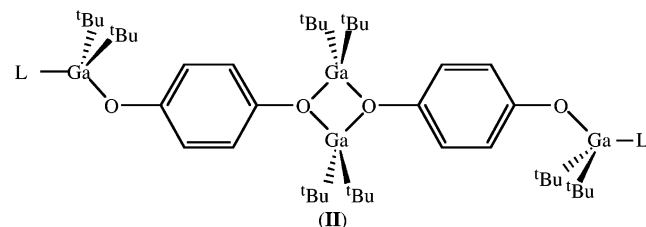


Table 1. Selected Bond Lengths (Å) and Angles (°) for [(*t*Bu)₂Ga(L)]₂(μ-OC₆H₄O) (**2–4**) and (*t*Bu)₂Ga(OPh)(py) (**5**)

compd	2	2.py	3	4	5
L	py	py	4-Mepy	3,5-Me ₂ py	py
Ga–O	1.836(3)	1.858(2)	1.849(3)	1.861(2)	1.875(2)
Ga–N	2.215(4)	2.112(3)	2.070(4)	2.075(3)	2.087(3)
Ga–C	1.921(5)	1.992(4)	1.971(5)	1.990(5)	1.990(4)
	2.082(5)	1.999(3)	1.989(4)	2.006(5)	1.998(4)
O–Ga–N	91.3(2)	96.9(1)	95.8(1)	92.6(1)	90.5(1)
O–Ga–C	101.7(2)	104.1(1)	105.3(2)	110.0(2)	109.2(2)
	119.9(2)	115.5(1)	115.2(2)	111.5(2)	113.0(2)
N–Ga–C	104.4(2)	103.1(1)	103.3(2)	103.3(2)	104.4(2)
	109.3(2)	106.7(1)	106.3(2)	106.9(2)	104.6(1)
C–Ga–C	124.4(2)	126.0(2)	126.0(2)	126.5(2)	127.8(2)
Ga–O–C	125.9(3)	128.3(2)	128.7(3)	127.1(2)	131.9(2)

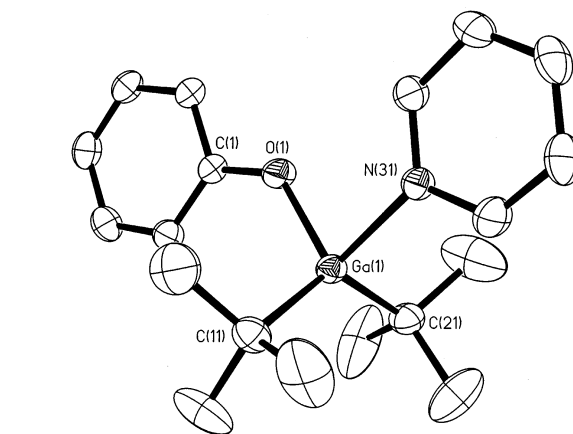


Figure 2. Molecular structure of [(*t*Bu)₂Ga(OPh)(py)] (**5**). Thermal ellipsoids shown at the 30% level, and hydrogen atoms are omitted for clarity.

Table 2. Thermodynamic Data for Ligand Dissociation from [(*t*Bu)₂Ga(L)]₂(μ-OC₆H₄O) (**2–4**) and (*t*Bu)₂Ga(OPh)(py) (**5**) in CDCl₃ Solution

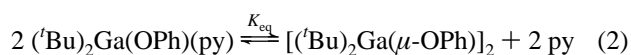
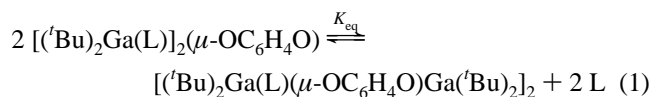
compd	L	K _{eq} @ 25 °C (mol·dm ⁻³) ^a	ΔH (kJ·mol ⁻¹) ^b	ΔS (J·K ⁻¹ ·mol ⁻¹) ^b	ΔG @ 25 °C (kJ·mol ⁻¹) ^b
2	py	1.48 × 10 ⁻⁴	69(2)	160(6)	21(2)
3	4-Mepy	2.98 × 10 ⁻⁴	52(2)	107(8)	20(4)
4	3,5-Me ₂ py	2.11 × 10 ⁻⁴	57(1)	125(2)	19(1)
5	py	1.45 × 10 ⁻⁷	103.2(3)	211.7(7)	40.1(5)

^a Calculated from thermodynamic data. ^b Errors given in parentheses.

This is in contrast to most dissociation equilibria observed for Group 13 Lewis acid–base complexes, including (*t*Bu)₂Ga(OPh)(py), which show a single set of resonances under equilibrium conditions.

The temperature dependence of the equilibrium constant allows for the determination of ΔH and ΔS using a Van't Hoff plot (Table 2). The ΔS values are positive, as would be expected for a dissociative process. The ΔH values are positive as well, indicating that this is an endothermic reaction, and the reactant is more stable than the product.

The ¹H and ¹³C NMR spectra of (*t*Bu)₂Ga(OPh)(py) (**5**) only show a single set of resonances under equilibrium conditions, but the ¹H NMR signals for the pyridine ligand of (*t*Bu)₂Ga(OPh)(py) have an upfield shift with increasing temperature.²⁰ The magnitude of the shift is temperature dependent consistent with the solution equilibrium shown in eq 2



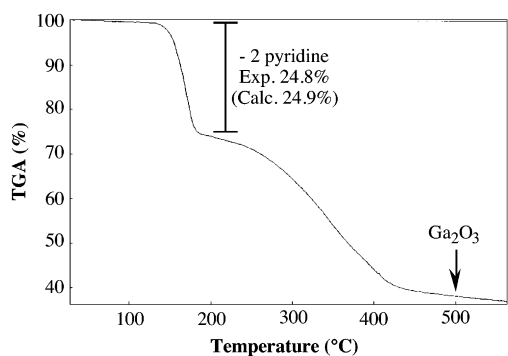


Figure 3. TGA of $[(t\text{Bu})_2\text{Ga}(\text{py})]_2(\mu\text{-OC}_6\text{H}_4\text{O})$ (**2**).

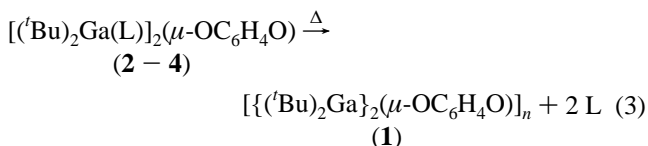
Table 3. Comparison of Powder XRD Data for $[(t\text{Bu})_2\text{Ga}]_2(\mu\text{-OC}_6\text{H}_4\text{O})_n$ Samples

reaction of $\text{Ga}(t\text{Bu})_3$ w. $\text{HOC}_6\text{H}_4\text{OH}$		thermal decomposition of $[(t\text{Bu})_2\text{Ga}(\text{L})]_2(\mu\text{-OC}_6\text{H}_4\text{O})$ (1) ^a	
2θ (°)	d	2θ (°)	d
11.48	7.70	11.38	7.77
12.38	7.14	12.29	7.19
13.29	6.66	13.10	6.75
14.40	6.15	14.40	6.15
18.20	4.87	18.42	4.81
25.29	3.52	25.37	3.51

^a FOM = 8.82 based upon a comparison with data from a sample prepared by the reaction of $\text{Ga}(t\text{Bu})_3$ with $\text{HOC}_6\text{H}_4\text{OH}$.

Assuming the ^1H NMR shift of the pyridine signal is directly proportional to the mole fraction of the total species present, the ^1H NMR chemical shift of the pyridine signals, at a given temperature, may be used to calculate the equilibrium constant, K_{eq} . The temperature dependence of K_{eq} allows for the determination of ΔH and ΔS for the reaction of eq 2 (Table 2).

Ligand Dissociation in the Solid State. The thermal decomposition of compounds **2–4** was studied in the solid state by thermogravimetric/differential thermal analysis (TG/DTA). Heating to 500 °C resulted in a weight loss, corresponding to the formation of Ga_2O_3 . Prior to this, an initial weight loss was observed starting at ca. 124 °C, which corresponds to the loss of 2 equiv of the Lewis base ligands; $\text{py} = 24.8\%$ (calc. 24.9%), 4-Mepy = 29% (calc. 28%), and 3,5-Me₂py = 28.8% (calc. 30.9%), e.g., Figure 3. A white stable material is formed after this initial weight loss and is confirmed to be $[(t\text{Bu})_2\text{Ga}]_2(\mu\text{-OC}_6\text{H}_4\text{O})_n$ (**1**) by ^{13}C CPMAS NMR spectroscopy and powder X-ray diffraction (Table 3). Furthermore, TGA/IR indicates that the only substance detected during that initial weight loss is the Lewis base. Thus, solid state thermolysis of $[(t\text{Bu})_2\text{Ga}(\text{L})]_2(\mu\text{-OC}_6\text{H}_4\text{O})$ yields $[(t\text{Bu})_2\text{Ga}]_2(\mu\text{-OC}_6\text{H}_4\text{O})_n$, eq 3



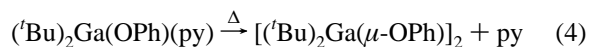
It should be noted that the dissociation of pyridine is not accompanied by melting. This may be observed visually in a melting point apparatus, where the color change from yellow to white is readily observed for a single crystal without

morphological change. Furthermore, no endotherm is observed in the differential thermal analysis (DTA) during pyridine loss.

The solid-state loss of pyridine from compound **2** has been followed by SEM and EDX. From point to point measurements of a single crystal before and after heating to 150 °C, there is a change in crystal volume with desorption of pyridine. A 26.6% decrease in volume is observed for the conversion of compound **2** to **1**. This should be compared a value of 25%, calculated from the atomic volume and the crystal density of compound **2** obtained from single-crystal X-ray diffraction.

Shown in Figure 4 are the SEM and the gallium and nitrogen EDX maps of a single crystal of $[(t\text{Bu})_2\text{Ga}(\text{py})]_2(\mu\text{-OC}_6\text{H}_4\text{O})$ along with the equivalent images for a sample after heating to 150 °C. Although the Ga EDX map shows a uniform composition, the N EDX map clearly shows the loss of nitrogen (i.e., pyridine) from the sample. As may be seen from Figure 4d, a single crystal of compound **2** appears to remain physically intact upon loss of pyridine. Unfortunately, we have been unable at this time to collect single-crystal diffraction data on compound **1**, despite the crystalline nature of the product (Table 3). We believe that this is associated with the formation of defects within the individual crystal and/or micro-cracks and porosity due to the loss of the volatiles. Support for this proposal is provided by surface area measurements. Solid-state loss of pyridine is accompanied by an increase in the surface area of the sample. BET measurements on a crystalline sample of compound **2** show a surface area of $0.098\text{ m}^2\cdot\text{g}^{-1}$. After careful heating to 150 °C to ensure dissociation of all the pyridine, and the formation of $[(t\text{Bu})_2\text{Ga}]_2(\mu\text{-OC}_6\text{H}_4\text{O})_n$, the surface area is increased to $0.688\text{ m}^2\cdot\text{g}^{-1}$.

The rate of loss of the Lewis base, and hence the conversion of $[(t\text{Bu})_2\text{Ga}(\text{L})]_2(\mu\text{-OC}_6\text{H}_4\text{O})$ (**2–4**) to $[(t\text{Bu})_2\text{Ga}]_2(\mu\text{-OC}_6\text{H}_4\text{O})_n$ (**1**) can be followed by TGA, and from the temperature dependence of the rate of mass loss (Figure 5), the ΔH^\ddagger and ΔS^\ddagger may be determined, Table 4. TGA-IR confirmed that pyridine is the only volatile product released under the conditions for which kinetic measurements were taken. The transformation of $[(t\text{Bu})_2\text{Ga}(\text{L})]_2(\mu\text{-OC}_6\text{H}_4\text{O})$ to compound **1** is clearly a dissociative process with a large positive ΔS^\ddagger , and the activation energies are within the range expected for the bond dissociation energy of a gallium Lewis base complexes with nitrogen donor.²¹ Solid state thermolysis of $(t\text{Bu})_2\text{Ga}(\text{OPh})(\text{py})$ (**5**) also results in the loss of 1 equiv of pyridine per gallium, and the residual white solid is confirmed to be $[(t\text{Bu})_2\text{Ga}(\mu\text{-OPh})]_2$ by ^1H NMR spectroscopy. As may be seen from Table 4, the values for ΔH^\ddagger and ΔS^\ddagger for the reaction described by eq 4 are significantly higher than compounds **2–4** (i.e., eq 3)



A comparison of ΔH^\ddagger (or ΔG^\ddagger) for the solid-state dissociation of L from $[(t\text{Bu})_2\text{Ga}(\text{L})]_2(\mu\text{-OC}_6\text{H}_4\text{O})$ (**2–4**) versus either the $\text{p}K_{\text{b}}$ (of L) or the Ga–N bond length, does not show any correlation. If we consider that ΔH^\ddagger might be dependent on the packing of the molecules, a comparison may be made with the distance between the two molecules that will subsequently form the dimeric core. A suitable measure is the Ga–Ga bond distance

(20) (a) Power, M. B.; Nash, J. R.; Healy, M. D.; Barron, A. R. *Organometallics* **1992**, *11*, 1830. (b) Healy, M. D.; Gravelle, P. W.; Mason, M. R.; Bott, S. G.; Barron, A. R. *J. Chem. Soc. Dalton Trans.* **1993**, 441.

(21) Barron A. R.; Power, M. B. Gallium: *Organometallic Chemistry*. In *Encyclopedia of Inorganic Chemistry*; King, R. B., Ed.; Wiley: Chichester, 1994.

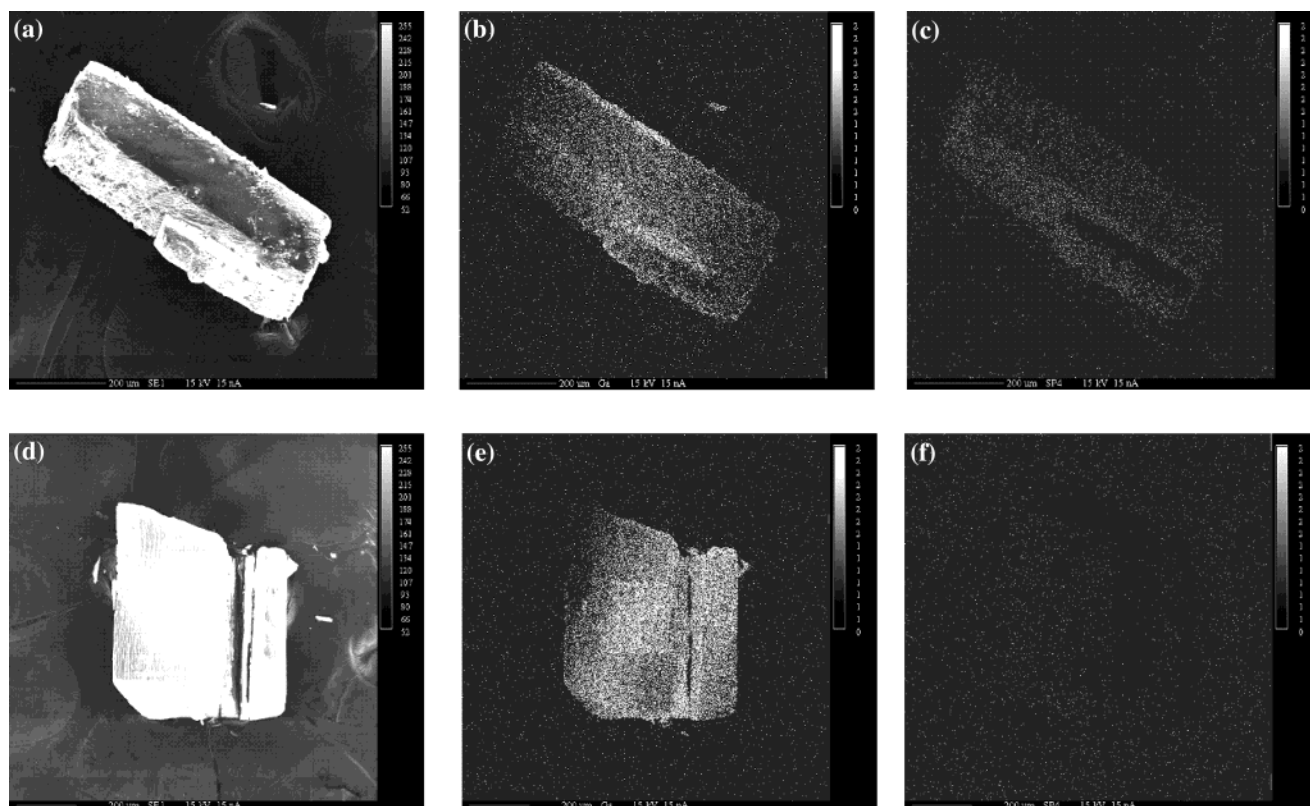


Figure 4. SEM (a, d) with associated gallium (b, e) and nitrogen (c, f) elemental maps of single crystals of $[(t\text{Bu})_2\text{Ga}(\text{py})]_2(\mu\text{-OC}_6\text{H}_4\text{O})$ (**2**) (a–c) along with the equivalent images for a sample after heating to 150 °C (d–f).

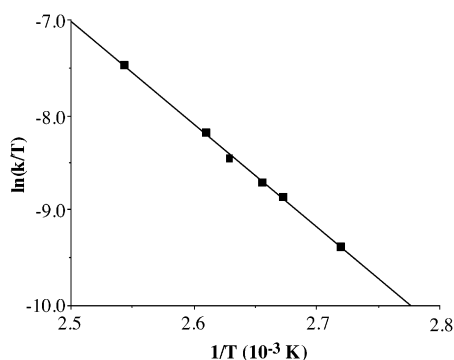


Figure 5. Plot of $\ln(k/T)$ as a function of $1/T$ for the conversion of $[(t\text{Bu})_2\text{Ga}(\text{L})]_2(\mu\text{-OC}_6\text{H}_4\text{O})$ (**2**) to $[(t\text{Bu})_2\text{Ga}(\text{L})]_n$ (**1**) ($R = 0.996$).

Table 4. Kinetic Data for Ligand Dissociation from $[(t\text{Bu})_2\text{Ga}(\text{L})]_2(\mu\text{-OC}_6\text{H}_4\text{O})$ (**2–4**) and $(t\text{Bu})_2\text{Ga}(\text{OPh})(\text{py})$ (**5**) in Solid State

compd	L	ΔH^\ddagger ($\text{kJ}\cdot\text{mol}^{-1}$) ^a	ΔS^\ddagger ($\text{J}\cdot\text{K}^{-1}\cdot\text{mol}^{-1}$) ^a	ΔG^\ddagger @25 °C ($\text{kJ}\cdot\text{mol}^{-1}$) ^a
2	py	96(3)	184(6)	41(1)
3	4-Mepy	66(2)	98(2)	36(1)
4	3,5-Me ₂ py	73(6)	125(17)	35(1)
5	py	126(1)	279(4)	42(1)

^a Error given in parentheses.

between two molecules in the asymmetric unit cell. As is shown in Figure 6, there exists a good correlation between ΔH^\ddagger (and ΔS^\ddagger) and the intermolecular Ga \cdots Ga distance for compounds **2**, **3**, and **5**. However, the 3,5-Me₂py compound (**4**) does not seem to follow the trend of the other compounds. The ΔH^\ddagger and ΔS^\ddagger values for compound **4** are much lower than would be

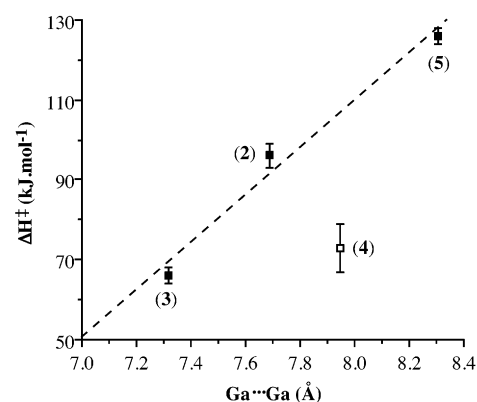


Figure 6. Plot of ΔH^\ddagger as a function of the intermolecular Ga \cdots Ga distance ($R = 0.979$).

expected when compared to the other compounds. Insight into this discrepancy can be obtained by examination of the crystal packing diagrams for compounds **2–5** (Figure 7).

Within the crystal unit cells of the pyridine (**2** and **5**) and 4-Mepy (**3**) compounds, the Lewis base ligands are arranged in a head-to-head fashion, meaning that the pyridine of one molecule is oriented toward a pyridine of another molecule next to it (see Figure 7a, b, and d). This packing motif requires that both molecules of pyridine must dissociate before dimerization can occur between the two fragments, such a process requires sequential dissociation of two Ga–N bonds, i.e., a dissociative–dissociative pathway (D,D), see Scheme 1. The relationship between the crystal packing and the ΔH^\ddagger (and ΔS^\ddagger) values for compounds **2**, **3**, and **5** is thus reasonable based upon a dissociative–dissociative (D,D), reaction pathway.

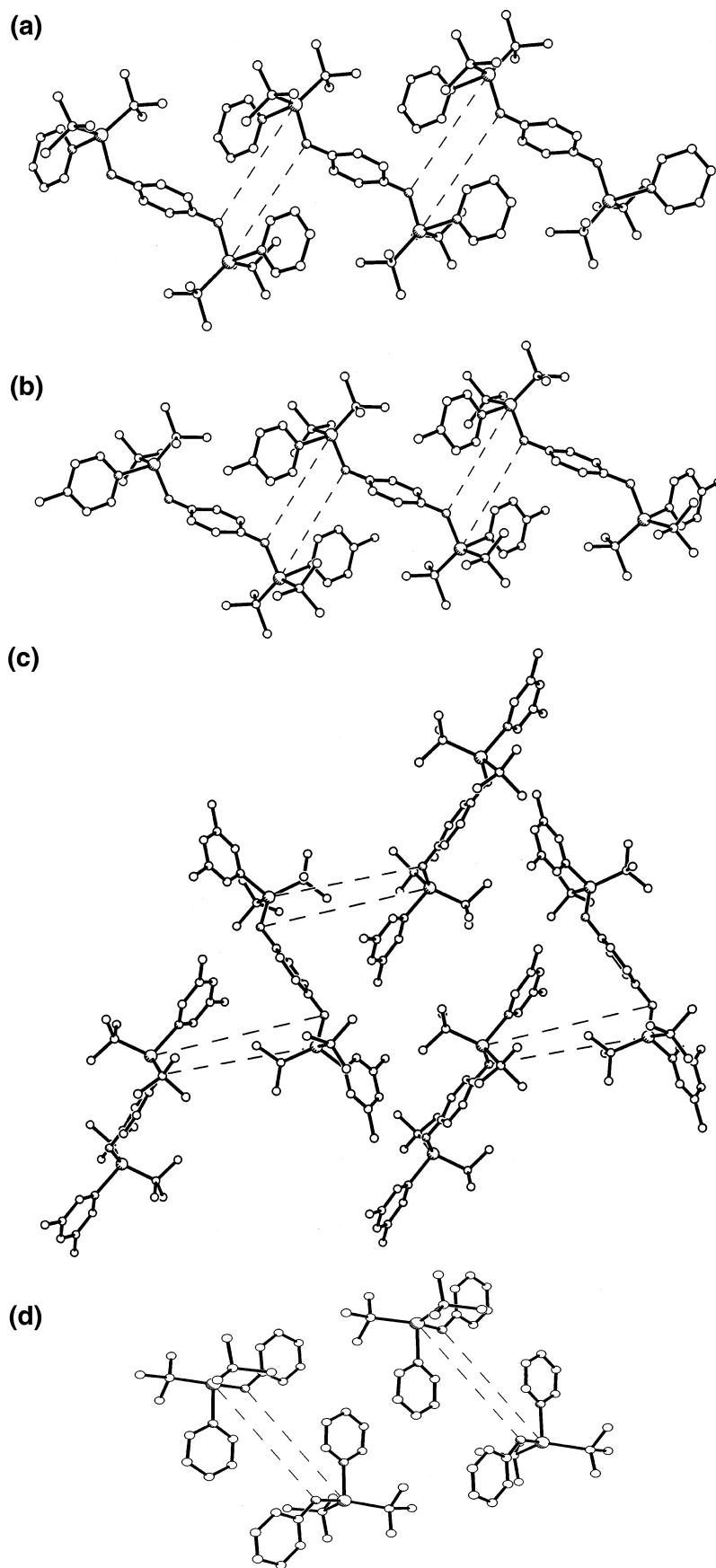
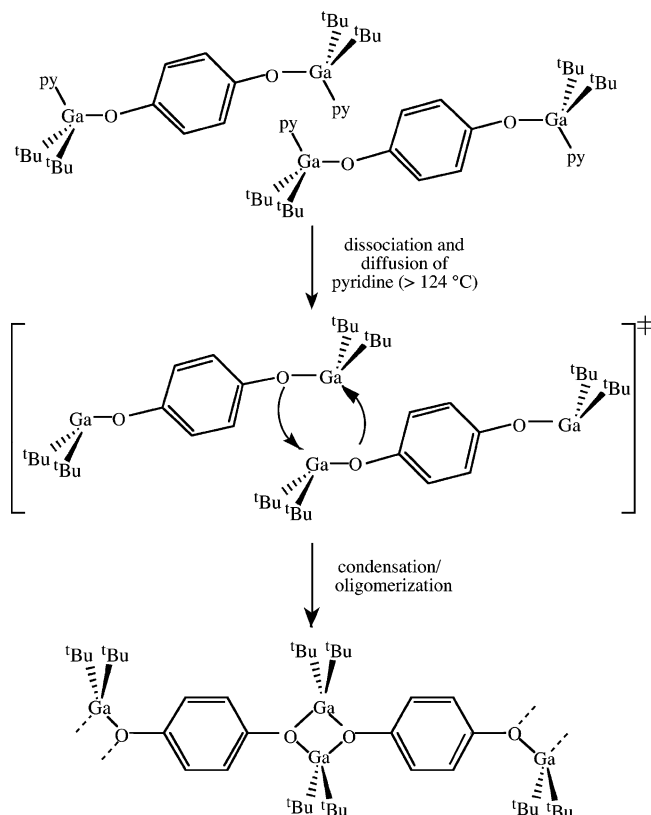


Figure 7. Crystal packing diagram for (a) $[(t\text{Bu})_2\text{Ga}(\text{py})]_2(\mu\text{-OC}_6\text{H}_4\text{O})$ (**2**), (b) $[(t\text{Bu})_2\text{Ga}(4\text{-Mepy})]_2(\mu\text{-OC}_6\text{H}_4\text{O})$ (**3**), (c) $[(t\text{Bu})_2\text{Ga}(3,5\text{-Me}_2\text{py})]_2(\mu\text{-OC}_6\text{H}_4\text{O})$ (**4**), and $[(t\text{Bu})_2\text{Ga}(\text{OPh})(\text{py})]$ (**5**) showing the relative position of the Ga–O units between adjacent molecules. Dashed lines indicate the vectors for Ga–O bond formation upon loss of the pyridine ligands. Ga...Ga bond distance 7.686 Å (**2**), 7.317 Å (**3**), 8.093 Å (**4**), and 8.308 Å (**5**).

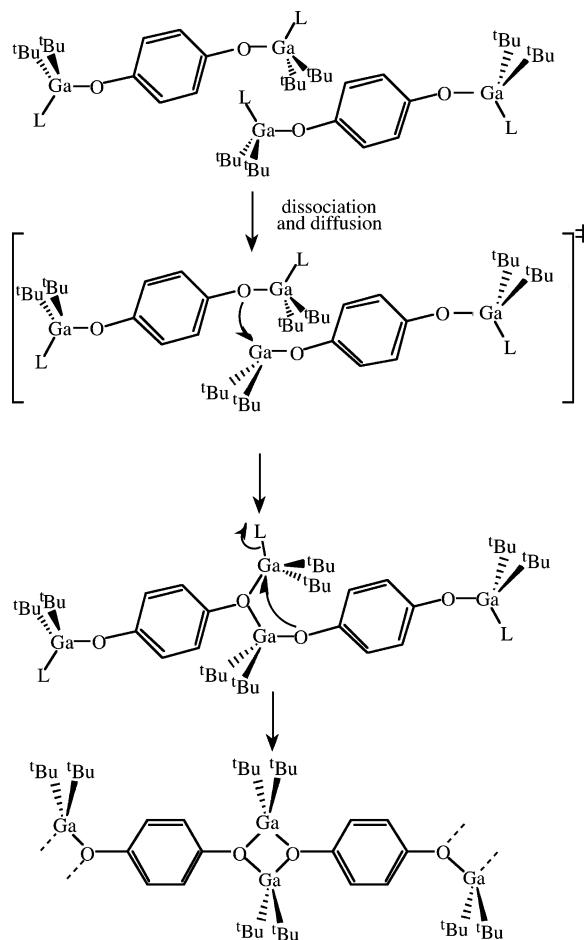
Scheme 1. Schematic Representation of the Thermal Conversion (D,D mechanism) of $(^t\text{Bu})_2\text{Ga}(\text{py})_2(\mu\text{-OC}_6\text{H}_4\text{O})$ (**2**) to $[(^t\text{Bu})_2\text{Ga}(\mu\text{-OC}_6\text{H}_4\text{O})]_n$ (**1**), Showing the Head-to-Head Orientation of One Molecule with Respect to Another



The crystal packing of compound **4** (Figure 7c) is quite different from the other derivatives; the molecules are oriented in a head-to-tail fashion. In this motif, the 3,5-Me₂py ligand on one molecule is oriented toward the gallium center of another (closest) molecule, and the ligand of 3,5-Me₂py on the second molecule points away from its nearest neighbor, see Scheme 2. This conformation allows for an alternative condensation pathway. The dissociation of one 3,5-Me₂py ligand allows for the association of the resulting coordinately unsaturated gallium center to the aryloxy center on an adjacent molecule. The remaining 3,5-Me₂py ligand may be substituted in an Associative (A) or Interchange (I) reaction step. It is reasonable to expect that the D,D mechanism would have a higher activation barrier than a D,A (or D, I) pathway, since the full dissociation of 2 equiv of the pyridine ligands are required for a single condensation. Such a rationale would explain the lower ΔH^\ddagger observed for compound **4** in comparison to the other homologues. If compound **4** crystallized out in a head-to-head polymorph it would be expected to have a larger ΔH^\ddagger for the loss of the 3,5-Me₂py ligands than observed in the head-to-tail polymorph. Although we have been unable to obtain single-crystal diffraction data (i.e., the Ga–Ga distance) for a head-to-head polymorph of compound **4**, we have shown that the head-to-head polymorph for does indeed have a significantly higher ΔH^\ddagger for the ligand dissociation/condensation reaction (as discussed below).

To provide further comparison between the D,D and D,A pathways, we have performed DFT calculations at the B3LYP level (see the Experimental section) on the model compounds: Me₂Ga(OMe), Me₂Ga(OMe)(NH₃), Me₂Ga(NH₃)(μ-OMe)-GaMe₂(OMe) (**III**), Me₂Ga(μ-OMe)(μ-Me)GaMe(OMe) (**IV**),

Scheme 2. Schematic Representation of the Thermal Conversion (D,A mechanism) of $(^t\text{Bu})_2\text{Ga}(3,5\text{-Me}_2\text{py})_2(\mu\text{-OC}_6\text{H}_4\text{O})$ (**4**) to $[(^t\text{Bu})_2\text{Ga}(\mu\text{-OC}_6\text{H}_4\text{O})]_n$ (**1**), Showing the Head-to-Tail Orientation of One Molecule with Respect to Another



and [Me₂Ga(μ-OMe)]₂ (**V**); selected calculated bond lengths and angles are given in Tables 5 and 6 along with comparative experimental values for related structures. A comparison with experimental values for *tert*-butyl analogues show a good agreement between experimental and calculated structural parameters.

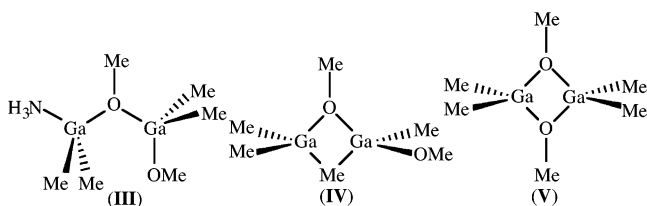


Figure 8 shows a calculated reaction diagram that simulates the dissociative–dissociative pathway proposed to occur for the condensation/polymerization reaction of compounds **2**, **3**, and **5** in the solid state. It should be noted that the overall reaction is endothermic ($-65 \text{ kJ}\cdot\text{mol}^{-1}$) rather than exothermic as is observed experimentally for the *tert*-butyl/pyridine derivative, see Table 2. This difference may be rationalized by considering the ΔH for dimerization. Upon the basis of the data in Tables 2 and 4, the ΔH dimer for compound **5** may be estimated to be $183 \text{ kJ}\cdot\text{mol}^{-1}$, which is significantly smaller than the value calculated for Me₂Ga(OMe), see Figure 8. This difference can be attributed to the steric bulk of the substituents (*tert*-butyl

Table 5. Selected Bond Lengths (Å) and Angles (deg) for Calculated Structures of Monomeric Gallium Alkoxides in Comparison to Experimentally Determined Values for Structural Analogs

compd	Me ₂ Ga(OMe)	(^t Bu) ₂ Ga(OCPh ₃) ^a	Me ₂ Ga(OMe)(NH ₃)	(^t Bu) ₂ Ga(OPh)(py) (5)
Ga–O	1.810	1.831(4)	1.880	1.875(2)
Ga–N			2.132	2.087(3)
Ga–C	1.920	2.003(6)	1.998	1.990(4)
	1.970	2.012(6)	1.998	1.998(4)
O–Ga–N			81.73	90.5(1)
O–Ga–C	118.6	115.0(2)	114.5	109.2(2)
	111.4	113.0(2)	114.4	118.2(2)
N–Ga–C			105.2	104.4(2)
			105.0	104.6(1)
C–Ga–C	130.0	126.1(2)	125.1	127.8(2)
Ga–O–C	125.9	127.5(3)	123.9	131.9(2)

^a Cleaver, W. M.; Barron, A. R. *Organometallics* **1993**, *12*, 1001.

versus methyl) and the alkoxide (OMe versus OPh).²² It is worth noting that as it should be, the ΔH dimer calculated for the formation of compound **1** is essentially independent of the identity of the Lewis base, i.e., ΔH dimer = 88 ± 3 , 80 ± 2 , and 89 ± 6 kJ·mol⁻¹ for compounds **2**, **3**, and **4**, respectively.

Figure 9 shows a reaction diagram representing the solid-state dissociative–associative pathway proposed to occur for the dimerization of compound **4**. The calculated dissociative–associative pathway shows that the activation barrier for the rate determining step (the dissociation of pyridine) is half that of the activation barrier for the dissociative–dissociative pathway. The experimental value for ΔH^\ddagger for **4** is 73% of the value expected for a dissociative–dissociative mechanism. Although not exact reproduction of the experimental observation, this trend is consistent with our experimental data.

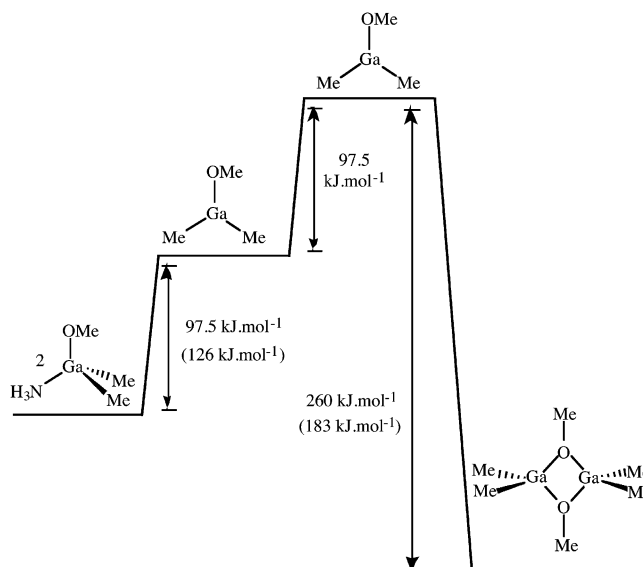
Ligand Association through a Solid/Vapor Reaction. Given that $\{[(^t\text{Bu})_2\text{Ga}]_2(\mu\text{-OC}_6\text{H}_4\text{O})\}_n$ (**1**) is converted to $[(^t\text{Bu})_2\text{Ga}(\text{L})]_2(\mu\text{-OC}_6\text{H}_4\text{O})$ (**2–4**) by dissolution in the appropriate ligand (or reaction with the appropriate ligand in hydrocarbon solution) and the reverse reaction occurs upon solid state thermolysis, we have investigated whether the interconversion of that $\{[(^t\text{Bu})_2\text{Ga}]_2(\mu\text{-OC}_6\text{H}_4\text{O})\}_n$ and $[(^t\text{Bu})_2\text{Ga}(\text{L})]_2(\mu\text{-OC}_6\text{H}_4\text{O})$ may be accomplished entirely in the solid state. The TG/DTA instrument was set up such that either N₂ or N₂/pyridine vapor could be used as the flow gas.

When a sample of $\{[(^t\text{Bu})_2\text{Ga}]_2(\mu\text{-OC}_6\text{H}_4\text{O})\}_n$ (**1**) is exposed to pyridine vapor at 34 °C a weight increase is observed equivalent to the uptake of one mole of pyridine per mole of gallium, i.e., the conversion of **1** to **2**. Confirmation of the formation of compound **2** in this manner may be obtained from powder XRD and solution and solid state NMR spectroscopy.

Table 6. Selected Bond Lengths (Å) and Angles (deg) for Calculated Structures and an Experimental Dimeric Gallium Alkoxide

compd	Me ₂ Ga(NH ₃)(μ-OMe)GaMe ₂ (OMe)	Me ₂ Ga(μ-OMe)GaMe ₂ (OMe)	[Me ₂ Ga(μ-OMe)] ₂	[(^t Bu) ₂ Ga(μ-OPh)] ₂ ^a
Ga–O _{br}	1.94, 1.99	1.95, 1.95	1.96, 1.95	2.035(1)
Ga–O _{ter}	1.90	1.82		
Ga–N	2.07			
Ga–C	1.98	1.98	1.98	1.993
O _{br} –Ga(1)–O _{br}			79.84	78.3(1)
O _{br} –Ga–N	94.9			
O _{br} –Ga–C	111.2, 108.5	109.4, 109.9	109.1, 108.9	107.2(2), 119.0(2)
C–Ga–C	125.8, 126.4	115.4, 129.2	129.9	119.6(5)
Ga–O _{br} –Ga	125.4	90.48	99.9, 100.3	101.7(1)
Ga–O _{br} –C	115.0, 120.2	125.2	123.7	129.1(1)
Ga–O _{ter} –C	119.4	—		

^a Cleaver, W. M.; McGuffey, A. R.; Bott, S. G.; Barron, A. R. *Polyhedron* **1994**, *13*, 2831.

**Figure 8.** Calculated reaction diagram for the dissociative–dissociative pathway proposed to occur for the condensation/polymerization reaction of compounds **2**, **3**, and **5** in the solid state. Experimental values for compound **5** given in parentheses.

The uptake of pyridine at a vapor pressure of 22 mmHg is rather slow, and whereas 95% uptake occurs in approximately 70 min., complete conversion of polymer **1** to compound **2** takes over 300 min. This observation is not surprising considering that the pyridine would react with the surface sites first and then have to diffuse further in the crystal lattice to find additional reactive sites. Switching the flow to pure N₂ and raising the temperature to 124 °C results in a mass loss equivalent to dissociation of the pyridine. The re-formation of **1** may be confirmed by powder XRD. Cooling to 34 °C and reintroducing the pyridine vapor again results in the formation of compound **2**. This process may be cycled repeatedly. The same result may be achieved by starting with $[(^t\text{Bu})_2\text{Ga}(\text{py})]_2(\mu\text{-OC}_6\text{H}_4\text{O})$ (**2**), e.g., Figure 10. It should be noted that the reformation of compound **2** appears to have a hysteresis; however, if sufficient time is allowed, then complete formation of **2** is attained. Alternatively, higher pyridine concentrations (through increasing the temperature of the pyridine bubbler and thus the pyridine partial pressure) diminish the hysteresis. It is important to note that powder XRD and ¹³C CP/MAS NMR indicate that decomposition is negligible after repeated association/dissociation cycles. Similar results have been found for compound **3**.

The rate of association of the Lewis base to the polymer varies with temperature. The temperature dependence allows for the

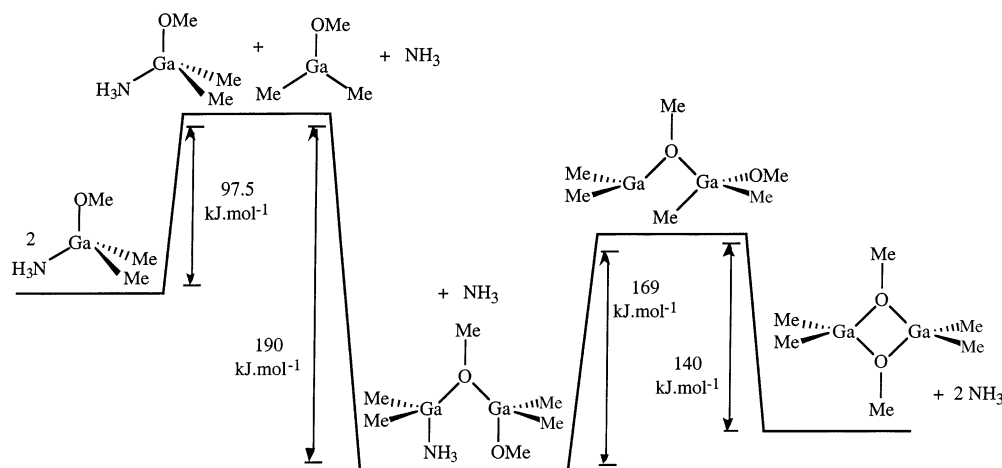


Figure 9. Calculated reaction diagram for the dissociative-associative pathway proposed to occur for the condensation/polymerization reaction of compound **4**.

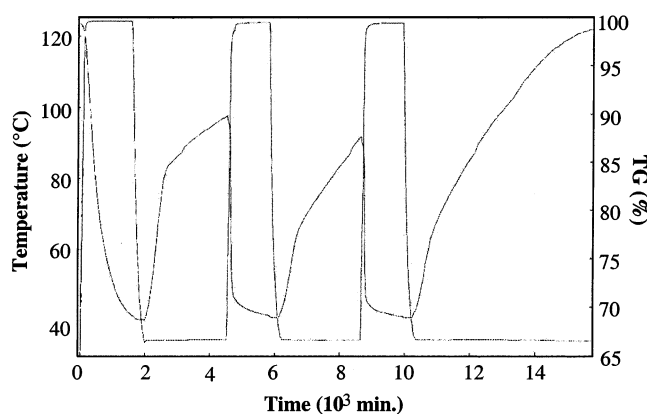


Figure 10. TG/DTA of $[(t\text{Bu})_2\text{Ga}(\text{py})]_2(\mu\text{-OC}_6\text{H}_4\text{O})$ (**2**) cycled under N_2 (124 °C) and $\text{N}_2/\text{pyridine}$ (34 °C) atmospheres, showing the reversible loss and uptake of pyridine. The hysteresis observed in the first and second cycles is obviated by the use of longer reaction times as is seen from the third cycle.

Table 7. Thermodynamic Data for the Formation of $[(t\text{Bu})_2\text{Ga}(\text{L})]_2(\mu\text{-OC}_6\text{H}_4\text{O})$ (**2** and **4**) from $[(t\text{Bu})_2\text{Ga}]_2(\mu\text{-OC}_6\text{H}_4\text{O})_n$ (**1**) Using the Solid State-Vapor Reaction

compd	L	ΔH^\ddagger ($\text{kJ}\cdot\text{mol}^{-1}$) ^a	ΔS^\ddagger ($\text{J}\cdot\text{K}^{-1}\cdot\text{mol}^{-1}$) ^a	ΔG @ 25 °C ($\text{kJ}\cdot\text{mol}^{-1}$) ^a
2	py	-168(3)	-553(3)	-3(2)
4	3,5-Me ₂ py	-167(3)	-560(2)	-1(2)

determination of ΔH^\ddagger and ΔS^\ddagger of the Ga_2O_2 dimeric core cleavage. These values are listed in Table 7 for the formation of compounds **2** and **4** from compound **1**.

It should be noted that with repeated cycles of association/dissociation of pyridine, i.e., $\mathbf{1} \leftrightarrow \mathbf{2}$, the ΔH^\ddagger does not change. This suggests that the same dissociative–dissociative (D,D) mechanism occurs through multiple cycles, and the structure of $[(t\text{Bu})_2\text{Ga}(\text{py})]_2(\mu\text{-OC}_6\text{H}_4\text{O})$ (**2**) is the same from one cycle to the next. To confirm this proposal, powder XRD was taken of $[(t\text{Bu})_2\text{Ga}(\text{py})]_2(\mu\text{-OC}_6\text{H}_4\text{O})$ (**2**) as it was crystallized out of solution and compared to that formed from the solid state–vapor reaction. A comparison of 2θ (°) and d spacing values for each sample confirms that the two samples have the same morphology (Table 8). Thus, the head-to-head polymorph is maintained

Table 8. Comparison of Powder XRD Data for Samples of $[(t\text{Bu})_2\text{Ga}(\text{py})]_2(\mu\text{-OC}_6\text{H}_4\text{O})$ (**2**) Showing Retention of the Crystalline Phase through Dissociation/Association Cycles

crystallization from solution		formation from vapor reaction w. $[(t\text{Bu})_2\text{Ga}]_2(\mu\text{-OC}_6\text{H}_4\text{O})_n$ (1) ^a	
2θ (°)	d	2θ (°)	d
11.10	7.96	11.21	7.88
12.37	7.15	12.29	7.19
13.02	6.79	13.06	6.77
16.10	5.51	16.11	5.50
19.22	4.62	19.22	4.61
29.96	2.98	29.99	2.98

^a FOM = 22.2 based upon a comparison with data from a sample of compound **2** crystallized from solution.

through repeated dissociation/association events for the solid state/vapor reactions.

If the addition of the Lewis base vapor to $[(t\text{Bu})_2\text{Ga}]_2(\mu\text{-OC}_6\text{H}_4\text{O})_n$ (**1**) gives $[(t\text{Bu})_2\text{Ga}(\text{L})]_2(\mu\text{-OC}_6\text{H}_4\text{O})$ in the head-to-head packing orientation, then we should see a change in the ΔH^\ddagger for the decomposition of $[(t\text{Bu})_2\text{Ga}(3,5\text{-Me}_2\text{py})]_2(\mu\text{-OC}_6\text{H}_4\text{O})$ (**4**) between the first and subsequent cycles. As we predicted above, the ΔH^\ddagger determined for $[(t\text{Bu})_2\text{Ga}(3,5\text{-Me}_2\text{py})]_2(\mu\text{-OC}_6\text{H}_4\text{O})$ (**4**) formed from the vapor–solid–state reaction of **1** with 3,5-Me₂py is indeed higher [88(7) $\text{kJ}\cdot\text{mol}^{-1}$] than that for a sample crystallized from solution [73(6) $\text{kJ}\cdot\text{mol}^{-1}$]. Furthermore, while we have been unable to obtain crystals suitable for single-crystal X-ray diffraction studies for the head-to-head polymorph for compound **4**, we can show that the crystal packing does change between the “as crystallized” samples and those formed from the solid–vapor reaction between compound **1** and 3,5-Me₂py. The formation of a new morphology is confirmed by powder XRD, see Table 9.

We propose, therefore, that when compound **4** is crystallized from solution a head-to-tail packing arrangement is formed, but during reintroduction of 3,5-Me₂py in the solid state/vapor reaction, a head-to-head polymorph is formed (i.e., the reverse of Scheme 1). Thus, the first and subsequent cycles form two different polymorphs with different activation barriers. If the ΔH^\ddagger for the second cycle onward, is compared to the ΔH^\ddagger versus Ga–Ga bond distance correlation for compound **4**, we see that the head-to-head polymorph is expected to have a Ga–Ga distance comparable to that observed for compound **2**.

(22) Francis, J. A.; McMahon, C. N.; Bott, S. G.; Barron, A. R. *Organometallics*, **1999**, *18*, 4399.

Table 9. Distinguishable Peaks Found for Powder XRD Data for Samples of $[(\text{tBu})_2\text{Ga}(3,5\text{-Me}_2\text{py})]_2(\mu\text{-OC}_6\text{H}_4\text{O})$ (**4**) Showing the Formation of Different Polymorphs Depending on the Synthetic Route

crystallization from solution		formation from vapor reaction w. $[(\text{tBu})_2\text{Ga}]_2(\mu\text{-OC}_6\text{H}_4\text{O})_n$ (1)	
2θ (°)	d	2θ (°)	d
10.08	8.77	9.94	8.88
10.79	8.19	10.57	8.36
11.48	7.70	11.61	7.62
11.87	7.45	14.81	5.98
16.59	5.34	17.17	5.16
28.50	3.13	28.29	3.15
		28.69	3.11

^a FOM = 0.23 based upon a comparison with data from a sample of compound **4** crystallized from solution.

In summary, the ΔH^\ddagger remains constant for the first and subsequent cycles of the dissociation of pyridine and 4-Mepy from $[(\text{tBu})_2\text{Ga}(\text{L})]_2(\mu\text{-OC}_6\text{H}_4\text{O})$ to $[(\text{tBu})_2\text{Ga}]_2(\mu\text{-OC}_6\text{H}_4\text{O})_n$ (**1**) and from $[(\text{tBu})_2\text{Ga}(\text{OPh}(\text{py}))]_2$ (**5**) to $[(\text{tBu})_2\text{Ga}(\mu\text{-OPh})]_2$. On the other hand, the first ΔH^\ddagger for the dissociation of 3,5-Me₂py to $[(\text{tBu})_2\text{Ga}]_2(\mu\text{-OC}_6\text{H}_4\text{O})_n$ (**1**) is different than that of subsequent cycles. As a result, we can conclude that the ΔH^\ddagger for the condensation polymerization reaction is dependent on the crystal packing (i.e., the Ga–Ga distance), and subsequently, the reversibility of the reaction is dependent on the polymorph.

Conclusions

The gallium aryloxide polymer, $[(\text{tBu})_2\text{Ga}]_2(\mu\text{-OC}_6\text{H}_4\text{O})_n$ (**1**) is synthesized by the addition of $\text{Ga}(\text{tBu})_3$ with hydroquinone, and reacts with pyridines, as both a solution and by a solid–vapor reaction, to yield the yellow compound $[(\text{tBu})_2\text{Ga}(\text{L})]_2(\mu\text{-OC}_6\text{H}_4\text{O})$ [$\text{L} = \text{py}$ (**2**), 4-Mepy (**3**) and 3,5-Me₂py (**4**)]. The energetics of the dissociation of one of the pyridine ligands in solution and solid state, and the association of the pyridine ligands by a solid–vapor reaction, provides insight into the reaction pathways for the interconversion of compounds **2–4** and compound **1**. Compounds **1** and **2** are reversibly interconverted without degradation or significant alteration in the reactivity or structure of the two components.

The polymorphism associated with sequential cycles for the 3,5-Me₂py derivative (**4**) is an interesting example of inducing pseudo-polymorphs via nonsolution methods,²³ for example, formation of new crystalline phases have been achieved by mechanical grinding and/or by thermal dehydration in thermogravimetric experiments. In this case, addition of a Lewis base vapor to a solid Lewis acid has formed a new polymorph with different thermodynamic barriers, than that made from the same addition in solution. Crystals of different polymorphs may be obtained via seeding, so the synthesis of this new polymorph might be achieved through seeding.

The color change (white to yellow) accompanying the conversion of compound **1** to **2** suggests that this or a similar process may be used as chemically triggered switches or chemical sensors. Although, clearly the present system is of limited practical value (due to the rate of switching and the application of pyridine) it does point the way to an alternative class of chemically triggered solid-state switches as opposed

to the more traditional inclusion compounds and compounds with vacant coordination sites. This study also suggests that in order for a sensor switch to be reversible, the same morphology (polymorph) must be maintained.

Experimental Section

Mass spectra were obtained on a Finnigan MAT 95 mass spectrometer operating with an electron beam energy of 70 eV for EI mass spectra. IR spectra (4000–400 cm⁻¹) were obtained using a Nicolet 760 FT-IR infrared spectrometer. Solution NMR spectra were obtained on a Bruker Avance 400 spectrometer. Chemical shifts are reported relative to internal solvent resonances. ¹³C CPMAS NMR spectra were recorded on a Bruker Avance 200 spectrometer. A 4 mm zirconium dioxide rotor was used for all spectra, with the spin rates up to 8 kHz. Microanalyses were performed by Oneida Research Services, Inc., Whitesboro, NY. Molecular weight measurements were made in CH₂-Cl₂ with the use of an instrument similar to that described by Clark.²⁴ Thermogravimetric/differential thermal analyses were obtained on a Seiko 200 TG/DTA instrument using a carrier gas of either dry nitrogen or air. TGA-IR was performed on a TA Instruments 2960 DTA-TGA connected to a Nicolet Nexus 670 FT-IR instrument. To enable powder XRD analysis, samples were mounted on glass slides by double sided tape prior to analysis. Data were collected on a Siemens D5000 diffractometer. Energy-dispersive X-ray spectroscopy (EDX) and scanning electron microscopy (SEM) were performed on a Cameca SX50 Electron Microprobe.

The synthesis of $\text{Ga}(\text{tBu})_3$ was performed according to a modification of the literature method.²⁵ $\text{HOC}_6\text{H}_4\text{OH}$, pyridine, 4-methylpyridine, 2,5-dimethylpyridine were obtained from Aldrich and (except for $\text{HOC}_6\text{H}_4\text{OH}$) were distilled and stored over Na metal prior to use. All manipulations were performed under an inert atmosphere of argon or nitrogen. Solvents were dried, distilled and degassed prior to use.

All density functional calculations were carried out using a Gaussian-98 suite.²⁶ Complete geometry optimizations were performed at B3LYP level using the 6-31G** basis set for C and H and Stuttgart RLC ECP basis set for Ga, N, and O.

$[(\text{tBu})_2\text{Ga}]_2(\mu\text{-OC}_6\text{H}_4\text{O})_n$ (**1**). Hydroquinone (0.522 g, 4.74 mmol) was suspended in degassed pentane and cooled to -78 °C. To this, $\text{Ga}(\text{tBu})_3$ (3.0 mL, 12.1 mmol) was added. The solution was allowed to warm to room temperature, and then was stirred for 1 day, giving a white powder. Yield: 1.2 g, 42%. ¹H NMR (d_5 -pyridine): δ 7.06 (4H, s, C_6H_4), 1.24 (36H, s, CH_3). ¹³C NMR (d_5 -pyridine): δ 156.7 (OC), 121.2 (OCCH), 31.4 (CH_3). ¹³C CPMAS NMR: δ 152.9 (OC), 120.8 (OCCH), 32.7 (CH_3).

$[(\text{tBu})_2\text{Ga}(\text{py})]_2(\mu\text{-OC}_6\text{H}_4\text{O})$ (**2**). **Method 1.** Hydroquinone (0.423 g, 3.8 mmol) was suspended in degassed pyridine and cooled to -78 °C. To this, $\text{Ga}(\text{tBu})_3$ (2.0 mL, 8.0 mmol) was added. The solution was allowed to warm to room temperature, and then was stirred for 1 day. The clear, yellow solution was cooled to -30 °C overnight, yielding crystals suitable for single-crystal X-ray analysis. Yield: 1.5 g, 62%.

(24) Clark, E. P. *Ind. Eng. Chem. Anal. Ed.* **1941**, *13*, 820.

(25) (a) Schwing, H. –U.; Jungk, E.; Weidlein, J. *J. Organomet. Chem.* **1975**, *91*, C4. (b) Kovar, R. A.; Derr, H.; Brandau, D.; Callaway, J. O. *Inorg. Chem.* **1975**, *14*, 2809.

(26) Frisch, M. J.; Trucks, G. W.; Schlegel, H. B.; Scuseria, G. E.; Robb, M. A.; Cheeseman, J. R.; Zakrzewski, V. G.; Montgomery, Jr., J. A.; Stratmann, R. E.; Burant, J. C.; Dapprich, S.; Millam, J. M.; Daniels, A. D.; Kudin, K. N.; Strain, M. C.; Farkas, O.; Tomasi, J.; Barone, V.; Cossi, M.; Cammi, R.; Mennucci, B.; Pomelli, C.; Adamo, C.; Clifford, S.; Ochterski, J.; Petersson, G. A.; Ayala, P. Y.; Cui, Q.; Morokuma, K.; Malick, D. K.; Rabuck, A. D.; Raghavachari, K.; Foresman, J. B.; Cioslowski, J.; Ortiz, J. V.; Baboul, A. G.; Stefanov, B. B.; Liu, G.; Liashenko, A.; Piskorz, P.; Komaromi, I.; Gomperts, R.; Martin, R. L.; Fox, D. J.; Keith, T.; Al-Laham, M. A.; Peng, C. Y.; Nanayakkara, A.; Challacombe, M.; Gill, P. M. W.; Johnson, B.; Chen, W.; Wong, M. W.; Andres, J. L.; Gonzalez, C.; Head-Gordon, M.; Replogle, E. S.; Pople, J. A., *Gaussian 98, Revision A.9*; Gaussian, Inc., Pittsburgh PA, **1998**.

(23) Braga, D.; Grepioni, F. *J. Chem. Soc., Chem. Soc. Rev.* **2000**, *29*, 229.

Table 10. Summary of X-ray Diffraction Data

compd	[(Bu) ₂ Ga(py)] ₂ (μ-OC ₆ H ₄ O) (2)	[(Bu) ₂ Ga(py)] ₂ (μ-OC ₆ H ₄ O) (2.py)
emp form	C ₃₂ H ₅₀ Ga ₂ N ₂ O ₂	C ₃₇ H ₅₅ Ga ₂ N ₃ O ₂
M _w	634.18	712.29
space group	P2 ₁ /c	P1
cryst system	monoclinic	triclinic
a, Å	8.705(2)	8.181(2)
b, Å	8.252(2)	8.525(2)
c, Å	24.736(5)	14.766(3)
α, °		106.21(3)
β, °	91.56(3)	99.01(3)
γ, °		95.64(3)
V, Å ³	1776.2(6)	965.7(3)
Z	2	1
no. collected	7603	4423
no. ind	2453	2765
no. obsd	(F _o > 4.0σ F _o)	2407 (F _o > 4.0σ F _o)
weighting scheme	SHELXTL 0.024, 0.00	SHELXTL 0.0535, 0.00
R ^a	0.0446	0.0404
R _w ^a	0.0886	0.0954
compd	[(Bu) ₂ Ga(4-Mepy)] ₂ (μ-OC ₆ H ₄ O) (3)	[(Bu) ₂ Ga(3,5-Me ₂ py)] ₂ (μ-OC ₆ H ₄ O) (4)
emp form	C ₃₄ H ₅₄ Ga ₂ N ₂ O ₂	C ₃₆ H ₅₈ Ga ₂ N ₂ O ₂
M _w	662.23	690.29
space group	P2 ₁ /c	P2 ₁ /n
cryst system	monoclinic	monoclinic
a, Å	8.683(2)	10.922(2)
b, Å	12.463(3)	14.052(3)
c, Å	16.935(3)	12.791(3)
α, °		
β, °	95.42(3)	94.33(3)
γ, °		
V, Å ³	1824.5(6)	1957.5(7)
Z	2	2
no. collected	8214	8746
no. ind	2635	2825
no. obsd	1613 (F _o > 4.0σ F _o)	2006 (F _o > 4.0σ F _o)
weighting scheme	SHELXTL 0.01, 0	SHELXTL 0.0531, 0
R ^a	0.0426	0.0416
R _w ^a	0.0741	0.1052
compd	[(Bu) ₂ Ga(OPh)(py)] (5)	
emp form	C ₁₉ H ₂₈ GaNO	
M _w	356.15	
cryst. syst.	monoclinic	
space group	P2 ₁ /n	
a, Å	14.972(3)	
b, Å	8.744(2)	
c, Å	16.182(3)	
α, °		
β, °	112.42(3)	
γ, °		
V, Å ³	1958.5(7)	
Z	4	
no. collected	8707	
no. ind.	2823	
no obsd	2120 (F _o > 4.0σ F _o)	
weighting scheme	SHELXTL 0.0661, 0	
R ^a	0.0379	
R _w ^a	0.0997	

$$^a R = \sum |F_o - F_c| / \sum F_o; R_w = \{ \sum [\{ w(F_o^2 - F_c^2)^2 \} / \{ w(F_o^2)^2 \}] \}^{1/2}.$$

Method 2. [({Bu)₂Ga}(₂(μ-OC₆H₄O))_n (0.15 g, 0.32 mmol) was dissolved in degassed pyridine and stirred for 1 day. The clear, yellow solution was cooled to -30 °C overnight, yielding yellow crystals. Yield: 0.17 g, 87%. ¹H NMR (CDCl₃): δ 8.98 [4H, d, J(H-H) = 4.0 Hz, NCH], 8.03 (2H, m, m-CH, py), 7.63 (4H, m, p-CH, py), 6.66 (4H, s, OCCH), 0.99 (36H, s, CH₃). ¹³C NMR (CDCl₃): δ 155.7 (OC), 148.5 (NCH), 140.1 (p-CH), 125.3 (m-CH), 120.8 (OCCH), 30.7 (CH₃). UV: λ = 329 (ε = 1200 L·mol⁻¹cm⁻¹), λ = 303 (ε = 4300 L·mol⁻¹cm⁻¹).

[({Bu)₂Ga(4-Mepy)]₂(μ-OC₆H₄O) (3). [({Bu)₂Ga}(₂(μ-OC₆H₄O))_n (0.15 g, 0.32 mmol) was dissolved in degassed 3,5-lutidine and stirred for 1 day. The clear, yellow solution was cooled to -30 °C overnight, yielding yellow crystals suitable for single-crystal X-ray analysis. Yield: 0.18 g, 86%. ¹H NMR (CDCl₃): δ 8.66 [2H, d, J(H-H) = 6.0

Hz, NCH], 7.43 [2H, d, J(H-H) = 6.0 Hz, m-CH], 6.62 (2H, s, OCCH), 2.53 (3H, s, CH₃), 1.04 [18H, s, C(CH₃)₃]. ¹³C NMR (CDCl₃): δ 158.8 (OC), 155.7 (NCH), 147.9 (p-CH), 126.3 (m-CH), 120.5 (OCCH), 30.9 [C(CH₃)₃], 23.4 (CH₃). UV: λ = 302 (ε = 5950 L·mol⁻¹cm⁻¹), λ = 327 (ε = 1500 L·mol⁻¹cm⁻¹).

[({Bu)₂Ga(3,5-Me₂py)]₂(μ-OC₆H₄O) (4). [({Bu)₂Ga}(₂(μ-OC₆H₄O))_n (0.15 g, 0.32 mmol) was dissolved in degassed 3,5-lutidine and stirred for 1 day. The clear, yellow solution was cooled to -30 °C overnight, yielding yellow crystals suitable for single-crystal X-ray analysis. Prepared in a manner similar to compound 2. Yield: 0.19 g, 87%. ¹H NMR (CDCl₃): δ 8.58 (2H, s, NCH), 7.64 (4H, s, p-CH), 6.65 (4H, s, OCCH), 2.44 (3H, s, CH₃), 0.99 [36H, s, C(CH₃)₃]. ¹³C NMR (CDCl₃): δ 155.7 (OC), 145.7 (NCH), 141.7(p-CH), 134.9 (m-CH), 120.6

(OCCH), 30.9 [C(CH₃)₃], 23.4 [C(CH₃)₃], 18.8 (CH₃). UV: $\lambda = 302$ ($\epsilon = 4050 \text{ L}\cdot\text{mol}^{-1}\text{cm}^{-1}$), $\lambda = 327$ ($\epsilon = 1600 \text{ L}\cdot\text{mol}^{-1}\text{cm}^{-1}$).

(^tBu)₂Ga(OPh)(py) (5). Phenol (0.195 g, 2.07 mmol) was suspended in degassed pyridine and cooled to -78°C . To this was added Ga(^tBu)₃ (0.5 mL, 2.1 mmol). The solution was allowed to warm to room temperature and stir for 1 day. The clear, yellow solution was cooled to -30°C overnight yielding crystals suitable for single-crystal X-ray analysis. Yield: 0.68 g, 90%. ¹H NMR (C₆D₆): δ 8.58 [2H, d, $J(\text{H}-\text{H}) = 5.0 \text{ Hz}$, NCH], 7.35 [2H, t, $J(\text{H}-\text{H}) = 5.0 \text{ Hz}$, *m*-CH], 6.89 [1H, t, $J(\text{H}-\text{H}) = 7.0 \text{ Hz}$, *p*-CH], 6.71 [1H, t, $J(\text{H}-\text{H}) = 7.0 \text{ Hz}$, *p*-CH, py], 6.40 [2H, t, $J(\text{H}-\text{H}) = 7.0 \text{ Hz}$, *m*-CH, py], 1.27 (18H, s, CH₃). ¹³C NMR (C₆D₆): δ 165.5 (OC), 148.4 (NCH), 139.8 (*p*-CH, py), 130.4 (*p*-CH), 125.3 (*m*-CH, py), 120.8 (OCCH), 117.6 (*m*-CH), 31.4 [C(CH₃)₃].

Solution Equilibrium Studies. Because a variation in ¹H NMR shifts for the α -methylene (OCH₂) is observed between different solvents, the same solvent (toluene-*d*₈) was used for all the variable temperature NMR measurements. The sample of each compound was heated to the appropriate temperature within the NMR spectrometer, and the ¹H NMR spectrum was collected. Constancy of the spectrum was taken as evidence for the attainment of equilibrium. The temperature of the NMR spectrometer probe was calibrated using the chemical shifts of ethylene glycol.²⁷ This process was repeated for a minimum of 6 temperatures over a minimum temperature range of 80 K. Alternate points on the $\ln K_{\text{eq}}$ versus $1/T$ plot were obtained during upward and downward passages over the temperature range spanned. Because both sets of points fell on the same line, we consider that equilibration was achieved. The temperature dependence of the equilibrium constant, K_{eq} , allows for the determination of the ΔH and ΔS . A summary of calculated values is given in Table 2.

Solid State Ligand Dissociation and Association Studies. Purified polycrystalline [(^tBu)₂Ga(L)]₂(μ -OC₆H₄O) [L = py (**2**), 4-Mepy (**3**), 3,5-Me₂py (**4**)] and (^tBu)₂Ga(OPh)(py) (**5**) were analyzed for volatility and thermal events on a thermogravimetric analyzer (Seiko TG/DTA 200). Typically 5–10 mg of sample were measured with heating rates of $10^\circ\text{C}\cdot\text{min}^{-1}$ up to 500°C under a $300 \text{ mL}\cdot\text{min}^{-1}$ inert (N₂ or Ar) gas flow. Isothermal mass loss was monitored over a 10 min period

before moving to the next temperature plateau. In all cases studied here, the mass loss at a given temperature was linear. The slope of each mass drop was measured and used to calculate dissociation enthalpies.²⁸ Association studies were performed by flowing the N₂ carrier gas through a pyridine bubbler (@ $300 \text{ mL}\cdot\text{min}^{-1}$). The sample (3–5 mg) was heated to between 34 and 44°C and the weight gain measured.

Crystallographic Studies. Single-crystal diffraction data for compounds **2–5** and **2.py** were collected at ambient temperature on a Bruker CCD SMART system, equipped with graphite monochromated Mo K α radiation ($\lambda = 0.71073 \text{ \AA}$) and corrected for Lorentz and polarization effects. The structures were solved using the direct methods program XS²⁹ and difference Fourier maps and refined by using full matrix least-squares methods. All non-hydrogen atoms were refined with anisotropic thermal parameters. Hydrogen atoms were introduced in calculated positions and allowed to ride on the attached carbon atoms [$d(\text{C}-\text{H}) = 0.95 \text{ \AA}$]. Refinement of positional and anisotropic thermal parameters led to convergence (see Table 10). In compound **2.py**, the lattice pyridine resides over a center of inversion, and so is statistically disordered. It was impossible to distinguish between different possible models of this disorder.

Acknowledgment. Financial support for this work is provided by the National Science Foundation and the Robert A. Welch Foundation, including the Bruker CCD Smart System Diffractometer of the Texas Center for Crystallography at Rice University. The Bruker Avance 200 NMR spectrometer was purchased with funds from ONR Grant No. N00014-96-1-1146.

Supporting Information Available: Full listings of bond length and angles, anisotropic thermal parameters, and hydrogen atom parameters; ¹³C CPMAS NMR spectrum of [(^tBu)₂Ga]₂(μ -OC₆H₄O)_{*n*}; van't Hoff plots for solution equilibria; Reaction diagram for ligand dissociation and dimerization of (^tBu)₂Ga(OR)(py); plot of ΔS^\ddagger as a function of the intermolecular Ga...Ga distance; calculated structures of Me₂Ga(OMe), Me₂Ga(OMe)(NH₃), Me₂Ga(NH₃)(μ -OMe)GaMe₂(OMe), Me₂Ga(μ -OMe)(μ -Me)GaMe(OMe), [Me₂Ga(μ -OMe)]₂. This material is available free of charge via the Internet at <http://pubs.acs.org>.

(27) (a) van Geet, A. L. *Anal. Chem.* **1968**, *40*, 2227. (b) Gordon H. J.; Ford, R. A. *The Chemists Companion*, Wiley, New York, 1972.

(28) Gillan, E. G.; Bott, S. G.; Barron, A. R., *Chem. Mater.* **1997**, *9*, 796.

(29) Sheldrick, G. M., SHELXTL. Bruker AXS, Inc. Madison, Wisconsin, **1997**.